ACS Biomaterials SCIENCE & ENGINEERING

pubs.acs.org/journal/abseba

Review

Particle-Based Microrheology As a Tool for Characterizing Protein-Based Materials

Michael Meleties, Rhett L. Martineau, Maneesh K. Gupta, and Jin Kim Montclare*

Cite This: *ACS Biomater. Sci. Eng.* 2022, 8, 2747−2763

Read Online

ACCESS | Metrics & More | Article Recommendations

ABSTRACT: Microrheology based on video microscopy of embedded tracer particles has the potential to be used for high-throughput protein-based materials characterization. This potential is due to a number of characteristics of the techniques, including the suitability for measurement of low sample volumes, noninvasive and noncontact measurements, and the ability to set up a large number of samples for facile, sequential measurement. In addition to characterization of the bulk rheological properties of proteins in solution, for example, viscosity, microrheology can provide insight into the dynamics and self-assembly of protein-based materials as well as heterogeneities in the microenvironment being probed. Specifically, passive microrheology in the form of multiple particle tracking and differential dynamic microscopy holds promise for applications in high-throughput characterization because of the lack of user interaction required while making measurements. Herein, recent developments in the use of multiple particle tracking and differential dynamic microscopy are reviewed for protein characterization and their potential to be applied in a high-throughput, automatable setting.

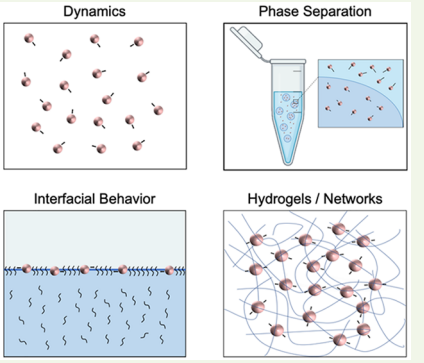

KEYWORDS: *microrheology, multiple particle tracking, differential dynamic microscopy, protein biomaterials, self-assembly*

INTRODUCTION

The characterization of mechanical properties is an important part of the materials discovery process. For soft and viscoelastic materials, rheological characterization yields important information about formulation characteristics and the performance of finished materials. Traditionally, rheological characterization has been performed by applying known stresses or deformations to a sample in bulk while monitoring the sample's response, typically one sample per instrument run.[1] Ideal elastic samples will respond completely in phase with the applied stress, whereas ideal inelastic samples (i.e., ideal Newtonian fluids) will respond completely out of phase with the applied stress.[2] In practice, most biomaterials display viscoelastic behavior that is characterized by a response between the two extremes.[2]

Since the turn of the century, microrheology has become an increasingly common method for characterizing viscoelastic behavior due to a number of advantages it possesses over traditional, bulk rheology.[3,4] Specifically, passive microrheology consists of tracking the movement of flow tracers, which can either be added in the form of inert tracer particles or be part of the system being investigated itself, and using information about the particle motion to determine local rheological properties of the medium.[5,6] One of the main advantages of microrheology is its use of a much smaller sample volume, using volumes as low as a few microliters, compared with bulk rheology, where the standard techniques typically require hundreds of microliters of material or more.[3,4,7,8] This is important for materials where sample preparation is a lengthy and/or costly process, as is often the case for protein-based materials. Additionally, because of the microscale sample sizes and the lack of physical contact required between the sample and the rheological instrumentation, microrheology based on multiple particle tracking (MPT) and differential dynamic microscopy (DDM) enables the analysis of numerous samples prepared in parallel and analyzed either sequentially or in an interleaved manner. For example, samples can be loaded into parallel microchannels[8] or in multiwell dishes[9] for easy optical probing. Because microrheology probes the microscale of the material, it is also able to uncover spatial heterogeneities that would otherwise be measured over and go unnoticed using standard rheology.[10] This is particularly useful for hydrogels that form as a result of physical cross-links and entanglements, such as many fiber-based protein hydrogels.[5,11,12]

Microrheology techniques can be classified as active or passive.[10] In active microrheology, a force is applied to tracer particles and the stress−strain relationship is then determined.

Received: January 11, 2022
Accepted: May 24, 2022
Published: June 9, 2022

https://doi.org/10.1021/acsbiomaterials.2c00035
ACS Biomater. Sci. Eng. 2022, 8, 2747−2763

This force can be generated through various different methods, including magnetic induction,[13] optical tweezers,[14,15] and atomic force microscopy.[16−18] Recent advancements in active microrheology have been reviewed and can be found here.[19−21] In passive microrheology, tracer particle motion is driven by the inherent thermal energy of the system.[10] The trajectories of the particles are optically measured and mean squared displacements (MSD) of the particles can be used to calculate the viscoelastic moduli of the medium using the generalized Stokes−Einstein relation.[10] The forces used in passive microrheology are extremely weak, enabling access to analysis regimes that are inaccessible to many bulk-scale rheology techniques.[7]

The role of microrheology in characterizing and understanding microscale dynamics has previously been reviewed for synthetic polymers and biopolymers,[22−26] but has yet to be reviewed exclusively for protein-based materials. Kastantin et al. have previously established the utility of single-molecule tracking, a qualitatively similar technique to MPT, in identifying interfacial dynamics between molecules and surfaces such as those that may occur at interfacial protein films.[23] Schultz and Furst meanwhile, have shown that MPT[27] can be streamlined for high-throughput use in the study of biomaterials.[22] With the recent development of DDM,[28−30] which consists of the same imaging done for MPT, we anticipate that high-throughput streamlining of MPT can easily be extended to DDM.

Protein-based biomaterials consist of a variety of macroscale structures and architectures such as fibers, micelles, and hydrogels.[31] These biomaterials often have properties that are dictated by their protein and peptide building blocks, including thermal transition properties and hierarchical self-assembly over time. Thus, an effective method that can characterize overall properties of the biomaterial—as well as local properties of the biomaterial—and relate them back to the individual building blocks would aid the design of next-generation biomaterials. Although we focus on the use of passive microrheology for the characterization of protein-based biomaterials, microrheology has also been used in other fields of soft matter including cosmetics chemistry, food science, and other polymer solutions and suspensions, where it has been used to characterize frequency-dependent viscoelastic properties and heterogeneities in the microstructure in order to determine ideal formulation conditions for different cosmetic and food products.[32,33] Herein, the use of passive microrheology methods to characterize the dynamics and self-assembly of protein-based materials is reviewed, with a focus on MPT and the more recently introduced DDM,[30] which have previously been evaluated in the context of polymer solutions[29] but have yet to be examined in the context of protein-based materials characterization. The use of these methods, especially in high-throughput, has the potential to accelerate understanding of protein-based materials, which can then be used to inform the design of novel biomaterials.

TECHNIQUES

Passive microrheology techniques track the movement of colloidal tracer particles typically on the scale of 0.1−10 μm and use the particle MSDs to extract properties of the material being studied. Data acquisition, in particular video microscopy of embedded tracer beads, is the same for both MPT and DDM; they differ in the way the image stacks are analyzed to determine MSDs (Table 1). Analysis through MPT is done in real space, tracking displacements of individual particles from frame to frame and then averaging over the ensemble, whereas DDM analysis is done in reciprocal space and averages over the entire image. In this section, MPT and DDM are discussed, as well as their advantages and limitations.

Table 1. MPT and DDM Differ in the Form of Their Analysis for a Series of Images with the Movement of Tracer Particles Being Tracked

MPT	DDM
• analysis in real space	• analysis in Fourier space
• user-defined inputs include particle-defining features such as intensity thresholds, size	• only user-defined input is normalized standard deviation cutoff
• tracks particle trajectories of individual flow tracers from frame to frame	• determines average mean squared displacement using intensity fluctuations across entire image space

Multiple Particle Tracking. MPT is a microrheological technique where noninteracting tracer particles are introduced into the medium or sample being studied and a series of images is recorded of particle movement, with trajectories tracked from frame to frame using particle intensity profiles (Figure 1). This makes it important for the particles to be resolvable in the images, indicating that the particles need to have high contrast and be optically dilute.[34] MPT algorithms require multiple user inputs that can have an effect on the data being counted toward ensemble statistics, including intensity profile thresholds, size of the features being tracked, maximum displacements from frame to frame, and the number of frames

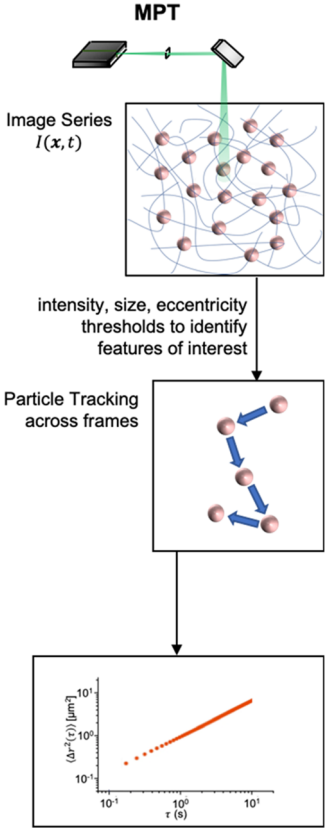

Figure 1. Workflow for passive microrheology using MPT. Series of images are taken for tracer particles in the sample. MPT analysis is done in real space, with user inputs used to isolate and track tracer particle trajectories.

https://doi.org/10.1021/acsbiomaterials.2c00035
ACS Biomater. Sci. Eng. 2022, 8, 2747−2763

a probe can skip in a long trajectory before being considered a different probe.[34−36] Restrictions set by the user can result in a significant fraction of measurements that would normally contribute to the ensemble average being discarded, which can lead to inaccurate results.

Advantages of MPT include revealing information on spatial heterogeneities within the sample, which can be assessed visually by looking at individual bead trajectories and how they compare to overall distribution of trajectories or quantitatively by calculating deviation from Gaussian behavior.[37,38] Furthermore, as MPT is much more established in the literature compared to DDM, MPT's bead-tracking algorithms are more developed, with dedrifting protocols already existing and easily applied,[34,39,40] whereas corrective algorithms for DDM have only recently been introduced.[41]

Differential Dynamic Microscopy Microrheology. DDM is one of the more recent optical microscopy-based microrheological techniques that has been developed.[30] Like MPT, DDM also involves the analysis of a series of images, but does so in the Fourier space (Figure 2). For each set of images, difference images are first generated by subtracting the intensity of each pixel in one image by the intensity of the same respective pixel in another image that is separated by a lag time (τ). The two-dimensional Fourier transform for each difference image can be decoupled into two contributions: the visual representation of scattering centers and the displacement of the scattering centers over different lag times. The dynamic image structure function, $D(q, \tau)$, which is a function of the wave vector (q) and lag time, is defined as the expectation value of the Fourier power spectrum of the computed difference images and can be broken down into three components.[28] $A(q)$ represents the Fourier transformed probe intensity profile, $B(q)$ represents incoherent background contributions, and $g(q, \tau)$, which is the equivalent of the autocorrelation function determined in dynamic light scattering (DLS), is dependent on the dynamics of the scatterer.[28] While the autocorrelation function has traditionally been used in DLS to characterize particle dynamics in solution and thus can also be used in DDM, Bayles et al. demonstrated how DDM analysis can be performed without fitting of the autocorrelation function, as $A(q)$ and $B(q)$ can be extracted from the image structure function as limits of the short- and long-term plateaus.[28,35]

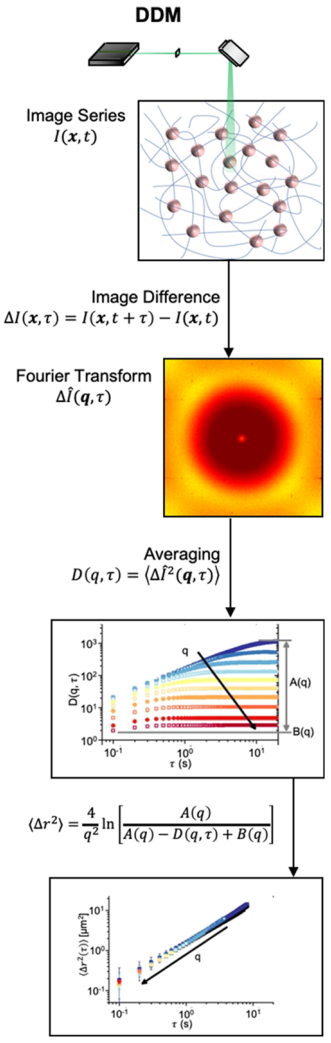

Figure 2. Workflow for passive microrheology using DDM. Series of images are taken for tracer particles in the sample. DDM analysis is done in the reciprocal space, with intensity fluctuations across the overall imaged space used to determine ensemble MSDs. The bottom two panels are reprinted with permission from ref 35. Copyright 2017 Springer Nature.

As lag time approaches zero, the intensity differences between images approaches a minimum, due to the scatterers not being expected to significantly change for a lag time of 0. This means that intensity fluctuations will be a result of the background noise and $B(q)$ can be taken as the limit of $D(q, \tau)$ as the lag time approaches zero, which can be approximated from the plot of $D(q)$ as $D(q, \tau_{min})$.[28] At long lag times, $D(q, \tau)$ reaches a plateau at a value that is the equivalent of $A(q)$ + $B(q)$, meaning $A(q)$ can now be extracted from the long-lag time plateau.[28] For noninteracting particles in a linear space invariant system, the MSD as a function of lag time can then be determined according to eq 1:

$$\langle \Delta r^2 \rangle = \frac{4}{q^2} \ln\left[\frac{A(q)}{A(q) - D(q, \tau) + B(q)}\right] \quad (1)$$

where $A(q)$ and $B(q)$ have been determined from the short- and long-lag time limits on the plot of $D(q, \tau)$ against τ.[35,42]

DDM has several advantages over more established microrheology methods such as MPT and diffusing wave spectroscopy (DWS). Unlike MPT, DDM scatterers do not have to be optically isolated or localized to be useful. This allows DDM to be used for the analysis of optically dense samples.[43] Additionally, DDM can be considered to be less user-dependent than MPT, with the only user input for DDM being a normalized standard deviation cutoff term.[35] DDM is easier to employ compared to DWS due to its use of unmodified microscopes that are commonly found in laboratories, whereas DWS requires specialized equipment.[28,30,35,44] DDM can be used in conjunction with various imaging modes including dark-field, bright-field, fluorescence, confocal, polarized, and phase-contrast microscopy,[28,35] furthering its ease of applicability in standard laboratories where one of these types of microscopes is likely to be in place. Like MPT, DDM has been shown to yield mechanical moduli of samples that agree with traditional rheology[42] in operating regimes where the techniques overlap in sensitivity. Importantly, image analysis by DDM can be optimized to the degree that user input and calibration are eliminated from the measurement process, enabling fully automated data analysis.[42]

https://doi.org/10.1021/acsbiomaterials.2c00035
ACS Biomater. Sci. Eng. 2022, 8, 2747−2763

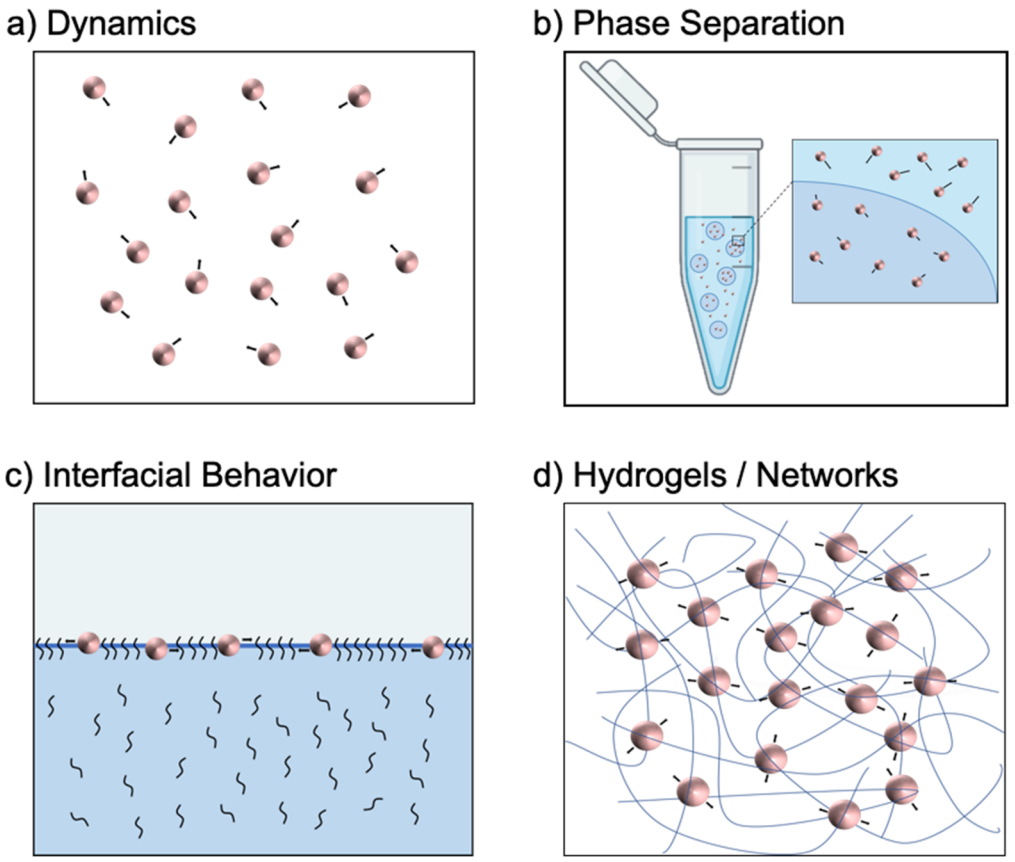

Figure 3. Application of passive microrheology for different systems. (a) Ability to track particle movement can be used to determine diffusivities and viscosities. (b) Heterogeneity during phase separation can be assessed using MPT, with different trajectory populations able to be determined in protein-rich and solvent-rich phases. (c) *In situ* measurements of passive microrheology can be used to assess interfacial behavior of proteins. (d) Tracking of particle movement over time can be used to assess hydrogel formation, with increasingly confined bead movement characteristic of an elastic medium.

MPT and DDM have already been used previously for high-throughput measurements. Schultz et al. used MPT to determine the optimal poly(ethylene glycol) (PEG) and high molecular weight heparin (HMWH) content and number of cross-linking sites for gelation of a PEG-HMWH system in a high-throughput screen.[8] In another study, Martinez et al. employed DDM to characterize the motility of different bacteria in high-throughput.[45] The distribution of swimming speeds and fraction of motile cells was extracted from videos of microbe motion observed over time spans of minutes, enabling multiple microorganism samples to be processed quickly.[45] Similarly, Jepson et al. have adopted DDM for determining the motility of bull spermatozoa in high-throughput.[46] Samples were placed in either disposable chambers or glass capillary tubes, imaged in rapid succession, and processed automatically using DDM.[46] In this case, the bull spermatozoa themselves are treated as noninteracting particles and diffusion is assumed to be the driving motion of nonmotile sperm.[46]

APPLICATIONS

Microrheology is useful in characterizing a variety of protein-based systems. DDM has thus far been mainly used for materials where tracer particles are undergoing Brownian motion, allowing particle-related properties such as diffusivities and medium-related properties such as viscosities to be determined (Figure 3a). MPT has been utilized to assess heterogeneous samples such as during phase separation and samples where tracer particle movement becomes impeded, such as in the formation of films and hydrogels (Figure 3b–d), whereas DDM has only recently started to be applied toward tracking of gelation. Examples discussed herein range from using microrheology in the form of MPT and DDM to determine properties related to dynamics of particles undergoing Brownian motion, tracking the unfolding of a protein in response to denaturants,[47] observing microrheological changes occurring in systems as proteins self-assemble into hydrogels, and using the locale-specific nature of MPT to identify regions within a sample with varied rheological properties as might be present during phase separation or formation of material interfaces such as liquid–air interfaces.[48]

Diffusion Coefficients. Microrheology is often used in determining the dynamics of a system, which includes characteristics such as particle diffusion coefficients or the microviscosities of the associated medium. The diffusion coefficient, D, is determined using the Stokes–Einstein relation (eq 2) for spherical particles diffusing in a low-Reynolds number liquid, where k_B is the Boltzmann constant, T is the temperature, η is the viscosity, and r is the radius of the particles.

$$D = \frac{k_B T}{6\pi\eta r} \tag{2}$$

In addition to being used to track inert particles, optical microscopy and particle-tracking techniques have been used to

https://doi.org/10.1021/acsbiomaterials.2c00035
ACS Biomater. Sci. Eng. 2022, 8, 2747–2763

determine the dynamics of microscale particles in biological environments. This becomes a limitation when dealing with particles on the nanoscale that are smaller than the resolution limit of brightfield microscopy. Fluorescent labeling of the particles has been previously touted as a solution, but this labeling can also alter the function and dynamics being measured.[49] DDM has been recently used by Safari et al. to determine the dynamics of weakly scattering and polydisperse protein-rich liquid clusters.[49] The diffusion coefficients and characteristic sizes of hemoglobin A and lysozyme are calculated on the basis of the diffusive relaxation times of their scattering wave vectors. The standard DDM fitting function of He et al. is modified to account for population polydispersity by introducing the factor $\mu\tau_c^2$, with μ being the second cumulant of the intensity-weighted diffusion coefficient and higher values of $\mu\tau_c^2$ indicating higher degrees of polydispersity.[49,50] The linear scaling of reciprocal relaxation times, $1/\tau_c$, with q^2 for both solutions indicate purely diffusive motion (Figure 4), with hemoglobin A and lysozyme having

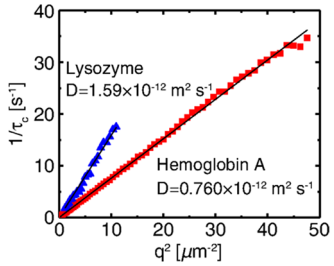

Figure 4. Reciprocal relaxation time as a function of wave vector for solutions of hemoglobin A (50 mg mL^{-1}) (red) and lysozyme (103 mg mL^{-1}) (blue). The linear fit of the reciprocal relaxation time passing through the origin indicates that motion is purely diffusive. Reproduced with permission from ref 49. Copyright 2015 American Physical Society.

diffusion constants of 0.760×10^{-12} and 1.59×10^{-12} m^2 s^{-1}, respectively.[49] Lysozyme solutions (0.16) are more polydisperse compared to hemoglobin A (0.075).[49] The characteristic radii determined through DDM are 232 nm for hemoglobin A and 95 nm for lysozyme, which are lower than the sizes of 144 and 72 nm for hemoglobin A and lysozyme, respectively, from DLS.[49] The discrepancy in the cluster sizes given by the two methods is attributed to the polydispersity of the cluster sizes; because of Mie scattering, as the cluster size distribution broadens, the size measured by DDM becomes progressively larger compared to the size measured by DLS.[49] Notably, this example displays one of the strengths of DDM relative to MPT, in that weakly scattering particles can be tracked based on intensity fluctuations rather than traditional frame-to-frame tracking that requires optical resolution of the particles. Additionally, DDM was shown to be useful in characterizing the size of polydisperse particles.

DDM was also used by Roth et al. to determine the diffusion coefficient of gold nanoparticles (NPs) in an alginate matrix, allowing them to develop a hybrid system where the peptidic E/K coiled-coil affinity pair is used for the release of nanoparticles.[51] NPs were functionalized with a cysteine-tagged Ecoil-epidermal growth factor (NP-CEE), whereas the alginate matrix was a mixture of unmodified and Kcoil-functionalized alginate through azide−alkyne cycloaddition (Alg-Kcoil), with 0, 10, or 20% of Kcoil-functionalized alginate used.[51] DDM was used to characterize the dynamics of functionalized and nonfunctionalized NPs (NP-CEE-PEG_{HD} and NP-PEG_{HD}, respectively) in the alginate matrix (Figure 5).

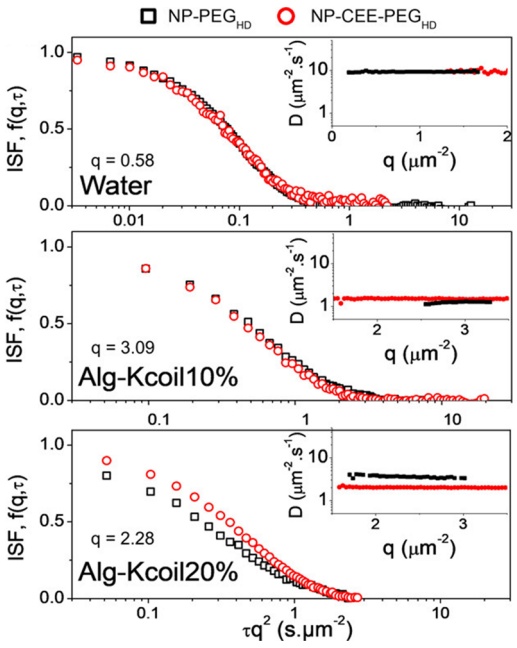

Figure 5. Intermediate scattering functions for gold nanoparticles functionalized with PEG (NP-PEG_{HD}, black) and gold nanoparticles functionalized with PEG and CEE (NP-CEE-PEG_{HD}, red) being tracked in three different media: water, Alg-Kcoil10%, and Alg-Kcoil20%. Insets show the diffusion coefficient of the particles in the respective medium, with q-values selected to best represent the short- and long-time plateaus of the intermediate scattering function. Reproduced with permission from ref 51. Copyright 2019 American Chemical Society.

At higher Kcoil-contents of alginate hydrogels, Ecoil-functionalized NPs had a higher retention in the matrix prior to release, with a diminished burst effect and retention increased by 20%.[51] Alternatively, in the lower Kcoil-content matrix, no discernible difference was observed between the Ecoil-functionalized NPs and nonfunctionalized ones.[51] This study demonstrates a unique use of DDM in characterizing the diffusivity of nanoparticles within a matrix as a proxy for affinity between nanoparticle and scaffold.

Viscosity. The viscosity of a protein solution can reveal key insights about protein stability and interactions. Notably, viscosity is affected by a variety of protein-related factors including the protein's net charge (i.e., pI and pH), the distribution of charge across the protein, hydrophobicity of the protein, and the protein's concentration.[52,53] The level of protein−protein interactions can thus be assessed by determining the viscosity of the solution, with microrheology a potential technique to accomplish this.[54] Escobedo-Sanchez et al. used DDM to measure the steady-sheer viscosity of a globular protein solution, among a total of three different materials: Newtonian fluids (water-glycerol mixture), colloidal samples (aqueous solution with globular protein (lysozyme)), and viscoelastic systems (poly(ethylene oxide)).[55] The results obtained agreed with independent measurements from DLS and oscillatory rheology. Results obtained for the lysozyme solutions showed that MSDs were right-shifted as the protein concentration increased, showing the role of increased protein−protein interactions (Figure 6).[55] Moreover, the

https://doi.org/10.1021/acsbiomaterials.2c00035
ACS Biomater. Sci. Eng. 2022, 8, 2747−2763

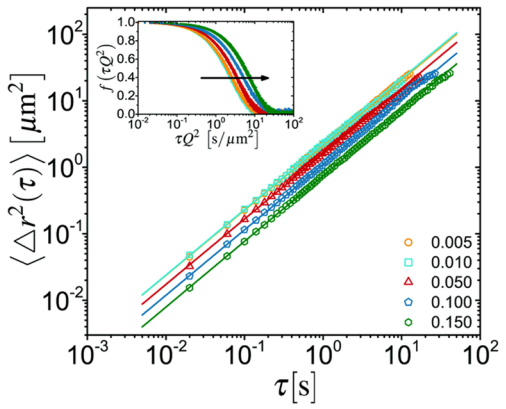

Figure 6. MSD as a function of lag time determined by DDM for 1.0 μm sized colloidal tracers coated with PEG in lysozyme solutions of different volume fractions. Inset shows the intermediate scattering function for the different volume fractions, with the arrow's direction indicating increasing volume fraction. Reproduced with permission from ref 55. Copyright 2018 The Royal Society of Chemistry.[55]

solution was confirmed to be purely viscous, with MSD showing a linear increase with respect to lag time.[55] These results are consistent with those obtained through other methods and underscore the capability of using a bright-field microscope as a viscometer. The advantages of using DDM to determine rheological properties such as viscosity using DDM include that frequencies up to 2 orders of magnitude lower than the limit of standard rheometers can be accessed using DDM, enabling a wider frequency range to determine the steady-shear viscosity.

Microrheology in the form of MPT was used to track differences in phase separation into liquid condensates by polylysine (polyK) and polyarginine (polyR) biopolymers of different lengths.[56] Furthermore, the polymer length effect on polyK liquid condensate properties was studied. Liquid droplets of polyK ranging from lengths of 10−100 monomers were able to form condensate droplets when combined with uridine phosphates (uridine-5′-triphosphate trisodium salt, UTP) or polyuridine (pU) of lengths 10 and 50. Higher-viscosity condensates were observed for higher polyK lengths, indicated by the lower MSD while maintaining a relaxation exponent consistent with Brownian motion (Figure 7).[56] For

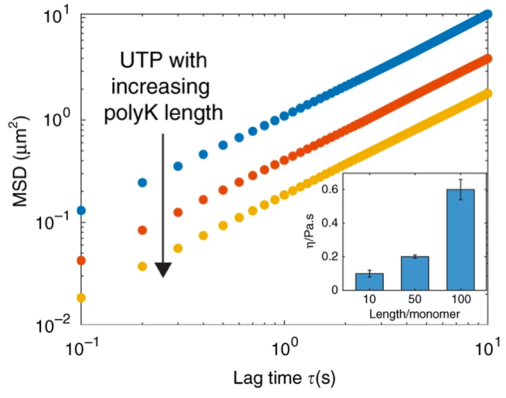

Figure 7. MSD of 0.5 μm-sized tracer particles in polyK/UTP droplets for varying polymer lengths of (blue) 10, (red) 50, and (yellow) 100 determined by MPT. Inset shows the viscosity of same droplets as a function of polymer length. Reproduced with permission from ref 56. Copyright 2020 Springer Nature.

polyK lengths of 10, 50, and 100, viscosities of 0.1, 0.2, and 0.6 Pa, respectively, were reported. Compared to polyK, where all polymer lengths were able to separate into liquid condensates, polyR was only able to form droplets with UTP at lengths of 10 and 50, while at lengths of 100 amorphous aggregates were reported. Notably, the viscosity of polyR droplets had viscosities 2 orders of magnitude higher than those reported for polyK, reaching 36 Pa for polyR10 and more than 200 Pa for polyR complexed with pU50.[56] This shows that, although the positive charge of the residues is conserved, the kinetics of liquid−liquid phase separation into condensates can be tuned by changing an amino acid. Considering that the viscosities of pure polyK and polyR are equivalent at concentrations up to 49.5 mg mL^{-1}, it is apparent that the complexation with nucleotides is key to shifts in the viscosity.[56] This is likely due to arginine being able to participate in $\pi-\pi$ interactions in addition to cation−π interactions, compared to cation−π interactions only for lysine.[56] This study demonstrates the utility of MPT, and microrheology as a whole, in determining viscosities of protein polymer solutions. Here, the viscosity is not only determined by using the MSD in conjunction with the Stokes−Einstein relation, but the lack of an elastic component is also confirmed by the relaxation exponent remaining equal to 1 for the different polyK lengths.

Interfacial Behavior. Because of their amphiphilic nature, proteins are likely to adsorb at air−water or oil−water interfaces, orienting themselves such that their hydrophilic domain faces the aqueous phase and the hydrophobic domain faces the air or oil phase.[57] The adsorption of proteins at these interfaces often results in the formation of viscoelastic layers or films, which lower the interfacial tension and have implications across a range of industries including food, cosmetics, and pharmaceuticals.[58] Thus, understanding the adsorption process resulting in protein film formation and how the mechanical properties at the interface evolve during adsorption would allow for more effective design of proteins for interfacial applications. Microrheology is an effective method to study adsorption at interfaces, with the movement of tracer beads over time being used to assess changes at the interface. Specifically, the *in situ* nature of microrheological measurements allow for effective monitoring of the system directly at the interface.[25]

MPT was used to study the interfacial behavior of native ß-lactoglobulin (ß-lg) and ß-lg aggregates in the forms of fibrils (F) and NPs at oil(decane)/water interfaces over time (Figure 8).[59] Briefly, the adsorption of protein aggregates at the oil/water consisted of a period of heterogeneity, with the final state representative of a uniform elastic protein film. Microrheology was useful in studying the adsorption process, providing an effective method to make *in situ* measurements of the microenvironment by assessing the relaxation exponent. A relaxation exponent of 1, meaning that the MSDs scale linearly with lag time, indicates that particles are undergoing Brownian motion.[38] As the material transitions from a solution to an elastic material such as a film or hydrogel, the relaxation exponent decreases to near 0 due to the particles having their movement impeded from the growing network.[38] Notably, in initial measurements all particles exhibited a relaxation exponent of 1 (Figure 8a), confirming their diffusive motion at the oil/water interface.[59] Over time, two distinct populations of tracer particles were observed—diffusive particles with relaxation exponents of 1 and another population with relaxation exponents <1, suggesting that their movement had

https://doi.org/10.1021/acsbiomaterials.2c00035
ACS Biomater. Sci. Eng. 2022, 8, 2747−2763

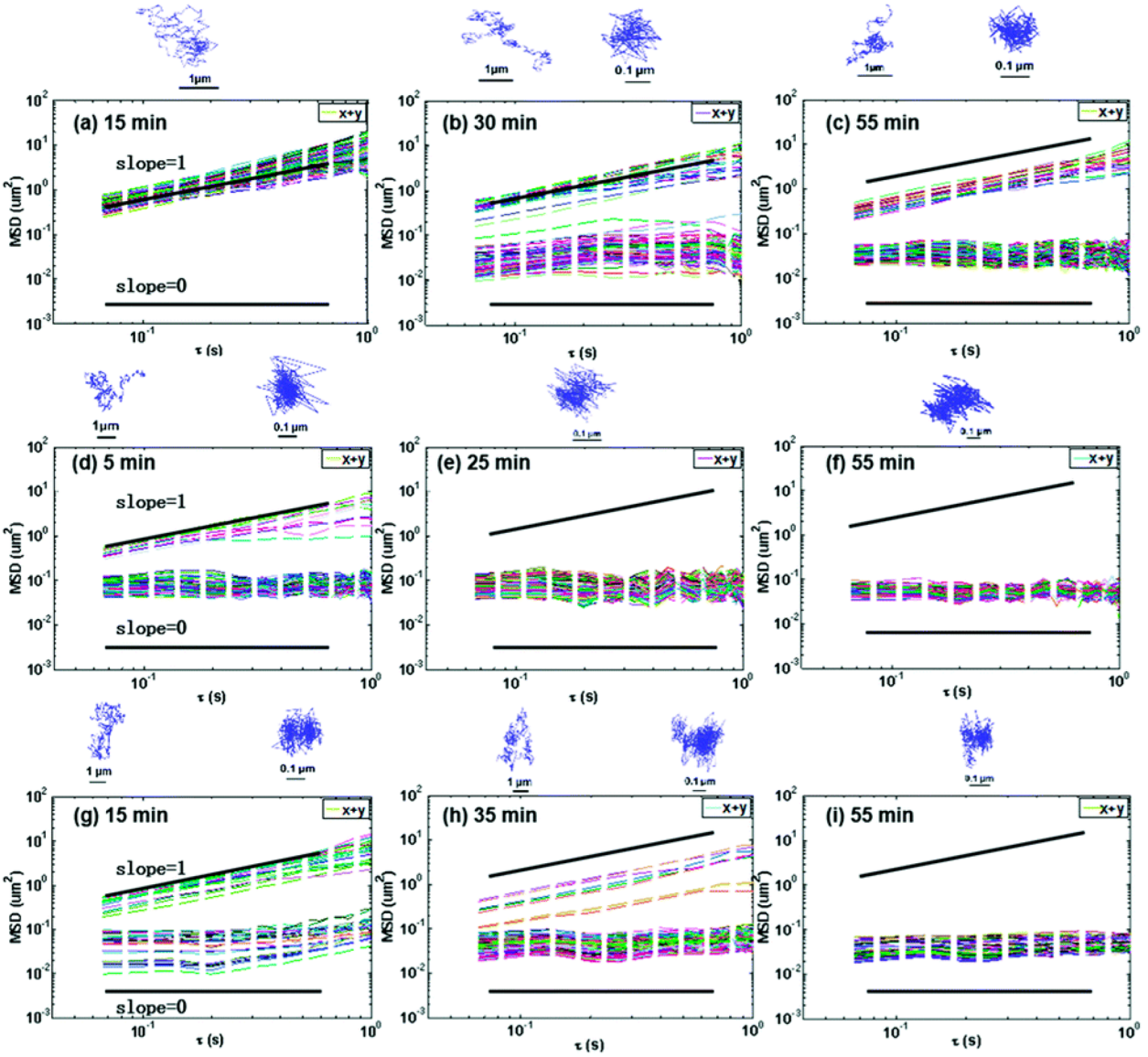

Figure 8. Individual MSDs of 1 and 0.1 μm sized tracer particles determined by MPT during protein adsorption at the oil/water interface from a 110 μg mL^{-1} solution. Time in each panel specifies the elapsed time since the formation of the interface for (a–c) ß-lg, (d–f) ß-lg NP, and (g–i) ß-lg F. Reproduced with permission from ref 59. Copyright 2021 The Royal Society of Chemistry.

started to become confined.[59] At the final observed time point, there were few particles that still had a relaxation exponent of 1, and most had transitioned to a relaxation exponent of 0, confirming that the final state of protein aggregates at the oil/water interface is an elastic film. Of the morphologies studied, ß-lg NP aggregates (Figure 8d–f) were reported to adsorb to the oil/water interface the fastest, followed by ß-lg F aggregates (Figure 8g–i), with ß-lg its native state (Figure 8a–c) showing the slowest rate of adsorption.[59] This specific example shows that microrheology is useful in assessing protein aggregation behavior at oil/water interfaces, highlighting the utility of *in situ* measurements by microrheology.

Self -Assembly and Gelation. Microrheology has also proved useful for its ability to identify key events in the self-assembly of proteins and peptides. As protein self-assembly can have various stages, microrheology can be used to identify differences on the microscale that accompany each step and analyze their kinetics.

Tu and Breedveld have previously shown that microrheology can be used to track the assembly of a globular protein, using MPT to track the unfolding of bovine serum albumin (BSA) due to the addition of a denaturant, urea.[47] Solution viscosities are determined for a range of urea concentrations by determining the MSDs for probe particles. A sigmoidal relationship is found between the solution viscosity and urea concentration (Figure 9a), consistent with the two-state model commonly employed in evaluating protein folding.[47] The unfolding midpoint determined through microrheology, 5.9 M, is comparable to the midpoint determined through spectroscopy of 6.4 M (Figure 9b).[47] The spectroscopically determined unfolding midpoint can be misleading as circular dichroism (CD) measurements can be affected by extremely stable secondary structures that remain even after the tertiary structure has unfolded.[47] The ability of microrheology to specifically track unfolding of the tertiary structure makes it an effective tool in tracking the self-assembly of globular proteins.

https://doi.org/10.1021/acsbiomaterials.2c00035
ACS Biomater. Sci. Eng. 2022, 8, 2747–2763

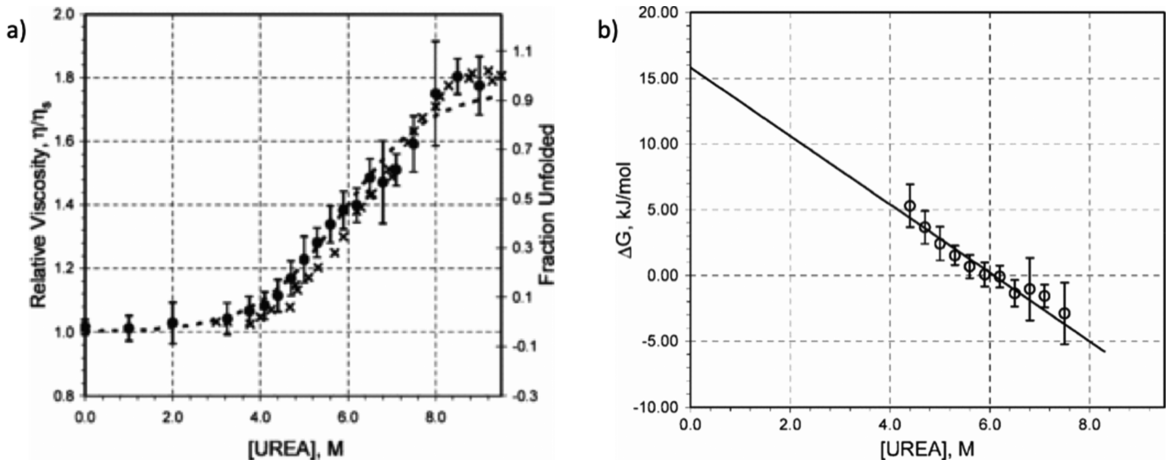

Figure 9. (a) Relative viscosity measurements of BSA as a function of urea concentration coincide with cooperative unfolding due to increased urea concentration. Viscosity measurements were made through MPT, using 1.0 μm-sized tracers. (b) Extrapolation of unfolding data gives estimate of free energy of unfolding ΔG = 15.5 ± 3.22 kJ mol^{-1}. Unfolding midpoint determined at urea concentration for ΔG = 0. Reproduced with permission from ref 47. Copyright 2005 American Physical Society.[47]

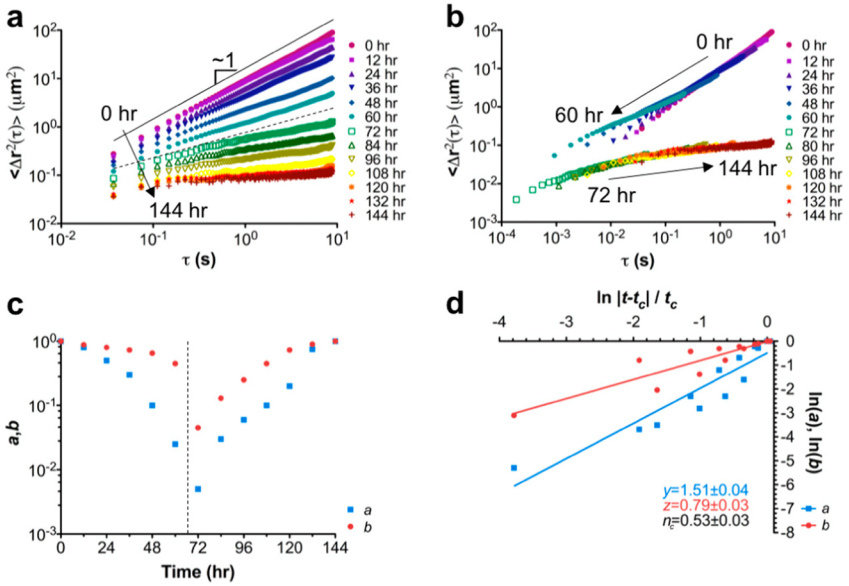

Figure 10. MPT used to track sol−gel transition of Q. (a) MSD−τ curves over time plotted for 1.0 μm sized tracer particles. (b) Time−cure superposition of MSD−τ curves. Intermediate curves were superimposed onto the master solution and master gel curves using horizontal and vertical shift factors. (c) Shift factors plotted with respect to time. Critical gelation time was determined from asymptotic behavior of the shift factors as they approached the critical extent of gelation. (d) Shift factors plotted against distance to critical gelation point on a logarithmic scale. The slope of the horizontal shift factors and vertical shift factors with respect to distance to critical gelation time (y and z, respectfully) are used to determine the critical relaxation exponent. Reproduced with permission from ref 11. Copyright 2019 American Chemical Society.

Microrheology is often employed in the assessment of soft biomaterials, such as hydrogels, which form from self-assembling monomeric units.[25] Specifically, the solution-to-gel (sol−gel) transition can be tracked by assessing the MSD-τ curves on a logarithmic plot over time.[25] The slope of these curves corresponds to the relaxation exponent and is normally between 0 and 1 for particles embedded in a material. Hill et al. used MPT to evaluate the sol−gel transition of a hydrogel based on the coiled-coil protein, Q (Figure 10).[11] Time−cure superposition, which consists of shifting intermediate MSD-τ curves on to the master solution (initial) and master gel (final) curve was done using horizontal (a) and vertical (b) shift factors, which scale the lag time and MSD, respectively (Figure 10b). The time at which the data diverges and is no longer superimposable onto the master solution curve can be considered the critical gelation time. Time−cure superposition revealed a sol−gel transition occurring for Q at 70.4 ± 0.1 h (Figure 10c), determined by plotting the shift factors over time and assessing the time at which asymptotic behavior of the shift factors was observed.[11] Comparing the slopes of the shift factors plotted with respect to distance from critical gelation time allows for the critical relaxation, n_c, to be determined, characterizing the degree of cross-linking in the system (Figure 10d). A critical relaxation exponent of 0.53 ± 0.03 was reported for Q, consistent with critical relaxation exponents reported for other physically cross-linked biomaterials.[5,6,11,60,61] Notably, tracking the evolution of tracer particle motion over time provides another efficient method to track gelation; specifically, this is useful for gelating systems whose phase transitions are not accompanied by changes in optical

https://doi.org/10.1021/acsbiomaterials.2c00035
ACS Biomater. Sci. Eng. 2022, 8, 2747−2763

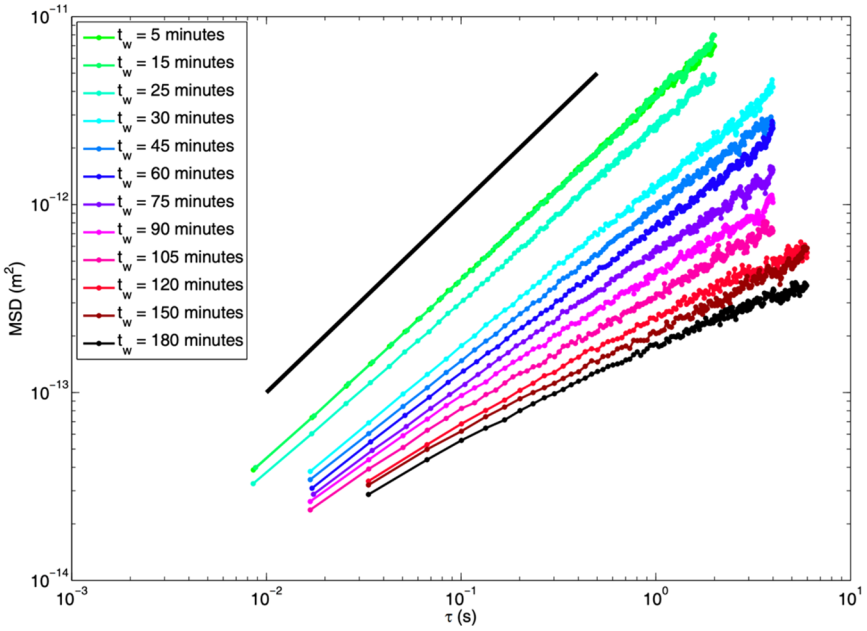

Figure 11. MSD with respect to lag time determined by MPT of 0.46 μm sized tracer particle evolution over time for a 10 mM Fmoc-Y sample with a GdL concentration of 10 mM. The behavior of tracer particles shifts from diffusive at earlier times to subdiffusive at latter incubation times. Reproduced with permission from ref 64. Copyright 2014 Springer Nature.

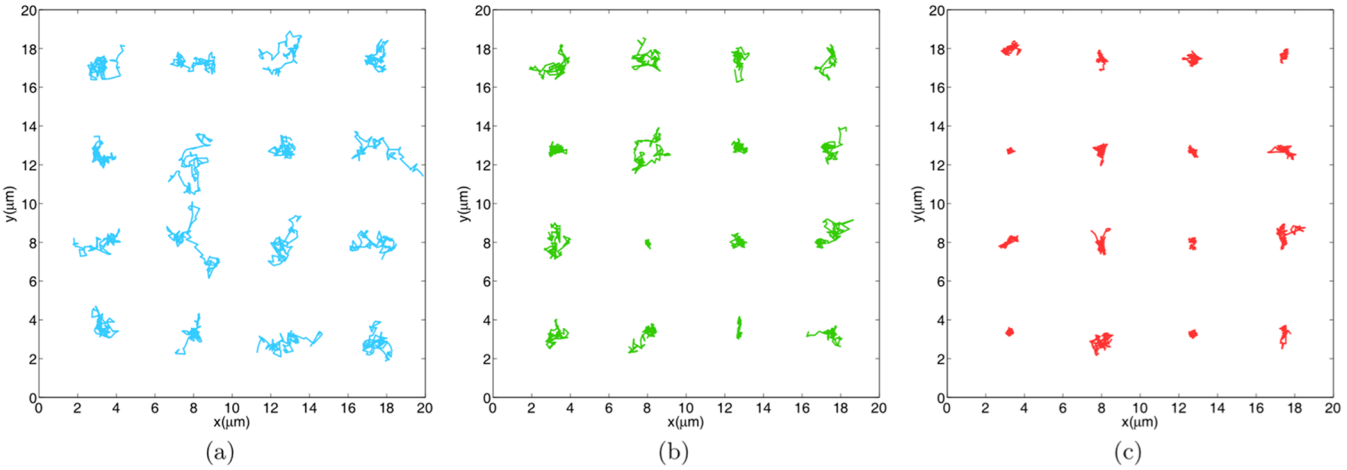

Figure 12. Representative probe particle trajectories for Fmoc-Y hydrogels gelled with GdL concentrations of (a) 5, (b) 7.5, and (c) 10 mM for 3 h. Trajectories of individual probe particles are plotted on a grid to reveal increasingly restricted motion with increasing GdL concentrations. A lack of uniformity in particle trajectories suggests heterogeneity in the hydrogel microenvironments. Reproduced with permission from ref 64. Copyright 2014 Springer Nature.

properties such as increasing turbidity. For systems with evolving optical properties during gelation, such as elastin-like polypeptide and silk-elastin-like polypeptide hydrogels,[62,63] DDM would be a preferred analysis method because its analysis is not required to be tuned to the system's specific optical properties.[28]

Aufderhorst-Roberts et al. utilized MPT to study the microrheology and microstructure of Fmoc-derivative hydrogels, specifically of Fmoc-tyrosine (Fmoc-Y).[64,65] MPT was used to track Fmoc-Y through its gelation process, which occurs as the result of the pH change brought on by the addition of glucono-d-lactone (GdL).[64] The time−cure superposition of MSD allowed for a critical gelation time and critical relaxation time to be determined, followed by the viscoelastic moduli. The kinetics and homogeneity of this gelation were further studied using MPT, with the MSDs of tracer particles being tracked over time (Figure 11). During the gelation reaction, a relaxation exponent of 1 was initially observed, indicating that the samples followed the behavior of Newtonian fluids at early extents of reaction.[64] As time passed, the magnitude of the MSDs began to decrease—although the power law exponent remained nearly 1—indicating an increase in the viscosity. Further forward, the logarithmic slope decreased below a value of 1 and, for more extreme extents of reaction, decreased as a function of lag time, confirming the subdiffusive behavior of the embedded particles and that the sample had transitioned into the gel state.[64] The final MSD was used to determine the equilibrium G' of the sample, which reasonably agreed with values from the literature. Microrheology is particularly useful in this example for its ability to characterize weak hydrogel networks, highlighting its ability to probe frequencies not accessible by oscillatory rheometry.

https://doi.org/10.1021/acsbiomaterials.2c00035
ACS Biomater. Sci. Eng. 2022, 8, 2747−2763

Investigation of the particle trajectories showed that for three different concentrations of GdL, 5, 7.5, and 10 mM, Fmoc-Y had heterogeneous microenvironments, which is shown by the lack of uniformity in the trajectories (Figure 12).[64] Although trajectories were not uniform, the probe particles appeared to be diffusing around fixed locations, consistent with how they would behave in a gelled system. Additionally, as GdL concentration increased, these trajectories became even more fixed, exhibiting a lower range of movements. Three different metrics, the heterogeneity ratio (HR), non-Gaussian parameter of the van Hove correlation function (N), and the bin distribution of the single particle MSD ($f(x)$), which is the ratio between the ensemble-averaged MSD of the fraction of particles with the highest MSD and the ensemble-averaged MSDs of all particles, were used to investigate the heterogeneity of the samples. Homogenous systems typically had particle displacements that follow a Gaussian distribution with a mean zero displacement.[37] To evaluate the heterogeneity of a system, the deviation from Gaussian behavior can be used as a metric. For the system reported by Aufderhorst-Roberts et al., all three metrics revealed an increase in heterogeneity following the gelation point, suggesting the microenvironments being probed by different particles were not consistent across the overall sample.[64] The work demonstrated the utility of MPT in characterizing the gelation kinetics of a system and the heterogeneity of the microstructure.[64] Perhaps more importantly, it demonstrates the use of three different metrics for assessing heterogeneity in a sample, opening up the possibility of using these metrics to compare different materials/experiments instead of only the same material under different conditions.

Levin et al. tracked the self-assembly of actin through the nucleation and elongation of actin filaments (F-actin) followed by network formation.[66] Although direct tracking of self-assembly is difficult because of the small size of actin filaments, MPT provided an indirect method of tracking self-assembly and network formation across a range of concentrations. Self-assembly kinetics dependent on the concentration of action monomers (G-actin) were reported, with concentrations above 2 μM yielding two transitions.[66] Prior to the onset of network formation, self-assembly was dominated by the loss modulus, whereas the storage modulus dominated at the end of self-assembly (Figure 13).[66] Considering actin filaments as stiff rods, lengths of the filaments were calculated at different points in the self-assembly process based on the effective viscosity of the system. Interestingly, distinct behaviors were observed for actin concentrations on either side of 4 μM. Below 4 μM, the elongation rate scaled with the cubic concentration, whereas elongation rate scaled linearly with concentration at actin concentrations greater than 4 μM.[66] This was consistent with low-concentration actin solutions having their elongation rate limited by the nucleation of the filaments, which requires 2−4 monomers, whereas high-concentration actin solutions are limited by the elongation process.[66] Notably, MPT is used in this example to track kinetics across multiple stages of actin self-assembly, demonstrating the ability to identify critical concentrations for self-assembly.

Meldrum et al. used MPT to investigate how the self-assembly of mucin is affected by components including mucin glycoproteins, nonmucin proteins, and Ca^{2+}-mediated links.[67] In screening a range of concentrations, a sharp decrease in the relaxation exponent was seen between 10 and 15 mg mL^{-1}

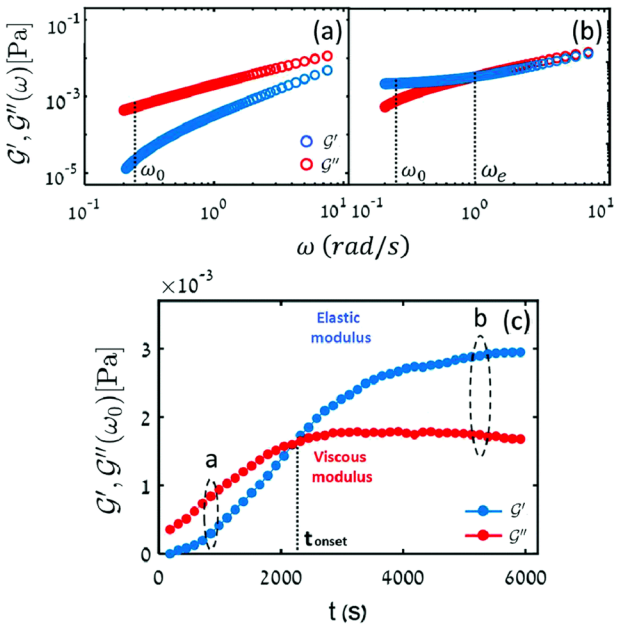

Figure 13. Self-assembly of actin networks for a monomer concentration of 3 μM assessed using viscoelastic moduli determine by MPT-based microrheology. 1.5 μm-sized polystyrene colloidal particles were tracked over time, with MSDs used to determine viscoelastic moduli of actin networks. (a) Near the beginning of self-assembly, G'' dominates G' over the 30 s interval the measurement is being made in. (b) Near the end of self-assembly, $G' > G''$ for the 30 s interval the measurement is being made in, representing an elastic network has formed. (c) G' and G'' tracked over entire self-assembly of actin network. Circled areas represent measurements from panels (a) and (b). Onset of elastic network formation, indicated by t_{onset}, is highlighted as the point where G' crosses over G''. Reproduced with permission from ref 66. Copyright 2020 The Royal Society of Chemistry.

(Figure 14). Interestingly, in the range of concentrations >15 mg mL^{-1}, diffusivity decreased steadily with concentration, but the relaxation exponent remained constant, suggesting an

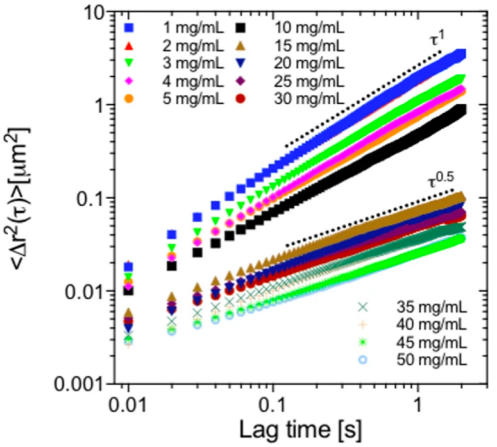

Figure 14. MSD of 0.5 μm sized tracer particles in mucin solutions of varying concentrations determined using MPT. Hyphened lines show scaling of MSD linearly with lag time and to a power of 0.5 with lag time. Notably, diffusive behavior was reported for concentrations ≤10 mg mL^{-1} and subdiffusive behavior was reported for concentrations ≥15 mg mL^{-1}. Reproduced with permission from ref 67. Copyright 2018 by Springer Nature.

https://doi.org/10.1021/acsbiomaterials.2c00035
ACS Biomater. Sci. Eng. 2022, 8, 2747−2763

increasing viscosity resulting in a gel-like fluid.[67] Under reducing conditions, mucin transitioned from having an elastic response to behaving more as a solution, indicating the importance of disulfide bonds in the initial mucin network.[67] Additionally, in the presence of the denaturant guanidine hydrochloride (GuHCl), similar effects were reported because of the loss of mucin structure.[67] Alternatively, network formation and elastic responses were favored in the presence of Ca^{2+}. Although addition of an equimolar amount of EDTA and Ca^{2+} led to similar behavior as mucin hydrogels, the addition of Ca^{2+} without EDTA led to an increased elastic response.[67] The addition of EDTA without Ca^{2+} resulted in a loss of elastic response.[67] Through the assessment of individual nonmucin components, losses in the elastic character of mucin were observed. Disruptions in multiple elastic-conferring components of the mucin network resulted in loss of elasticity, confirming a mechanism for network formation that is dependent on synergistic contributions from multiple components.[67] MPT is again used here to elucidate the hierarchical mechanism of assembly of mucin hydrogels, with Ca^{2+} links forming following the effects of other interactions, such as hydrogen bonding.

Joyner et al. also employed MPT to track the gelation of mucin-based hydrogels mediated by hydrogen bonding and disulfide bond formations, focusing on the effects of cross-linkers with different degrees of thiol-functionalization.[68] Briefly, thiolized 10 kDa PEG cross-linkers (PEG-1SH, PEG-2SH, PEG-4SH) and thiolized dextran (dextran-SH, 10 kDa) were studied for their ability to cross-link porcine gastric mucin (PGM).[68] MSDs of tracer particles were tracked both immediately after mixing (0 h) and after 9 h.[68] Of the thiolized PEG cross-linkers used, only PEG-4SH exhibited decreases in the relaxation exponent consistent with gelation (Figure 15).[68] Alternatively, no change in relaxation exponent

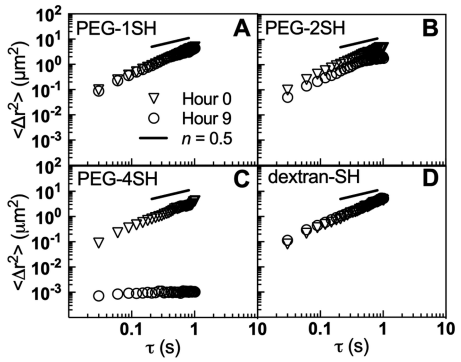

Figure 15. MSD of 0.1 μm sized tracer particles in mucin mixed with different thiolized cross-linkers, including (A) PEG-1SH, (B) PEG-2SH, (C) PEG-4SH, and (D) dextran-SH. MSDs, were determined by MPT analysis. Measurements were made at 0 h (triangles) and 9 h (circles), with lines having a slope of 0.5 included for reference. Reproduced with permission from ref 68. Copyright 2019 The Royal Society of Chemistry.

was reported for PEG-1SH, because of the lack of cross-linking by only containing a single thiol group per PEG, and PEG-2SH showed a slight decrease in the relaxation exponent, consistent with some degree of cross-linking but not to the extent to form a hydrogel.[68] A possible reason for the decrease in MSD was the increase of effective polymer weight following disulfide bond formation with PEG-2SH.[68] Cross-linkers with a dextran backbone were also not reported to form hydrogels, with the authors speculating that this was due to the rigidity of the backbone compared to PEG.[68] The disulfide bond-dependent nature of the hydrogel matrix was further confirmed through the addition of the reducing reagent N-acetyl cysteine (NAC) to already-formed PGM hydrogels, with network breakdown reported in 30 min.[68] Similarly, treatment of PGM with iodoacetamide (IAM) led to its alkylation, which effectively blocked cysteines in the PGM and thus inhibited hydrogel formation.[68] MPT was used to confirm the mediation of mucin-based hydrogels by hydrogen bonds and disulfide linkages.

Yonemoto et al. utilized MPT to investigate the mechanism of formation for multichannel collagen gels (MCCG) and uncover heterogeneities in the microstructure.[69] In this work, *in situ* microrheological measurements were made throughout the gelation process, with gelation occurring following bulk flow of a collagen solution in the sample. A collagen concentration- and pH-dependent gelation mechanism was elucidated. At 3.0 mg mL^{-1} collagen, no gelation was observed at pH 6, whereas at pH greater than 6.5, the relaxation exponent was near 0, indicating an elastic gel.[69] Following gelation of the MCCG, three different populations of particle relaxation exponents behavior were reported: particles with near-zero relaxation exponents, which were deemed to be trapped in the gel, particles that displayed Brownian motion and were thus still freely diffusing in the channels, and particles whose relaxation exponents were characteristic of an intermediate viscoelastic behavior (Figure 16).[69] Although most particles showed behavior consistent with being confined in a gel, a clear population of particles with behavior consistent of a fluid-like medium was also observed.[69] This was confirmed using confocal laser scanning microscopy (CLSM), revealing collagen-rich elastic phases and solvent-rich dilute phases (Figure 16). The variation of relaxation exponents during MCCG formation at short and long lag time regions was used to assess mechanism and homogeneity. In the short lag time region, particles in the elastic gel demonstrated a sharp decrease in relaxation exponent consistent with elastic solids, whereas the relaxation exponent for particles in the capillary regions of the gel remained at 1, characteristic of Brownian motion in solutions. Furthermore, relaxation exponents in the long lag time region revealed an increase over time, suggesting a bulk motion associated with these particles. This was correlated to the rapid spinodal decomposition that occurred, with particle movement showing the formation of two distinct phases.[69] MPT was utilized to make *in situ* rheological measurements, with its ability to track individual beads useful for probing and identifying different phases within the overall scaffold.

Zhou et al. have employed MPT as a means to track the self-assembly of π-conjugated oligopeptides across a range of concentrations.[48] The system being investigated consists of a π-conjugated oligopeptide with a quarterthiophene (OT4) core, HO-DFAG-OT4-GAFD-OH (DFAG-OT4), which assemble into ß-sheet-rich fiberlike structures at neutral pH. Sampled probe trajectories are shown to be described well by Gaussian statistics, indicating that the sample being studied is homogeneous.[48] When tracking the MSD as a function of concentration, two shifts are observed. Fickian diffusion, characteristic of Newtonian solutions, is observed at low concentrations, indicating minimal self-assembly.[48] As the concentration increases past 0.1 mg mL^{-1}, the relaxation

https://doi.org/10.1021/acsbiomaterials.2c00035
ACS Biomater. Sci. Eng. 2022, 8, 2747−2763

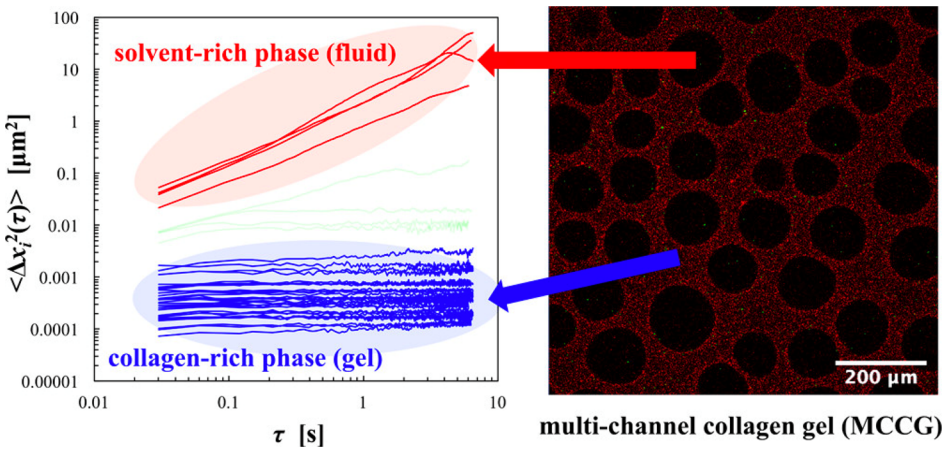

Figure 16. (Left) 0.49 μm sized particle MSDs in MCCG corresponding to (right) CLSM imaging of MCCG determined by MPT. Trajectories were representative of multiple particle populations probing different microenvironments. Particles showing a linear increase in MSD with respect to lag time (red) were prevalent in solvent-rich phases, indicated by the red arrow, whereas particles showing a constant MSD with respect to lag time (blue) were prevalent in the continuous collagen-rich gel phase, indicated by the blue arrow. Reproduced with permission from ref 69. Copyright 2021 American Chemical Society.

exponent decreases from 1, indicating subdiffusive behavior (Figure 17a). This shift to subdiffusive behavior is attributed to the onset of self-assembly, with emerging fibers causing a change in the local microenvironment and hindering particle movement.[48] As the concentration is increased past 1 mg mL^{-1}, the relaxation exponent further decreases (Figure 17a).[48] This is explained by the onset of gelation from the physical entanglement of the fibers, further hindering the movement of the probe particles. The critical gel concentration, c_{gel}, is confirmed to be 1 mg mL^{-1} through time−cure superposition (Figure 17b).[48] The critical relaxation exponent, a_{crit}, is determined to be 0.78, with the relaxation exponent further decreasing to approximately 0.5 for concentrations greater than c_{gel}.[48] This value suggests a fully percolated gel network has formed through fractal polymer growth, which is in keeping with previous studies on fiber-based systems.[12,48] MPT was combined with optical spectroscopic techniques such as circular dichroism to determine critical concentrations for fiber formation and gelation while tying them to structural changes occurring for the oligopeptides.

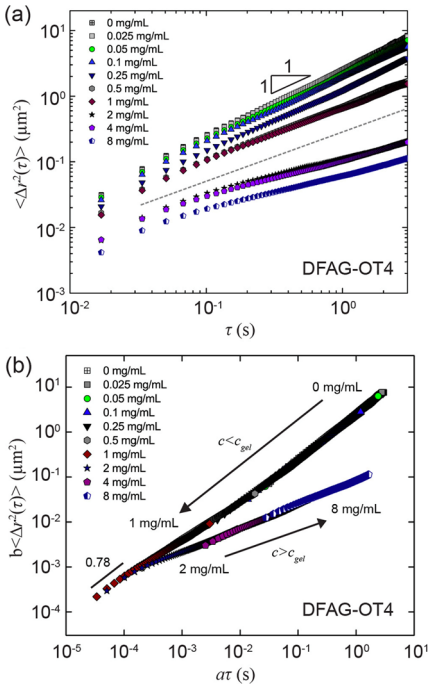

Figure 17. Sol−gel transition of DFAG-OT4. (a) MSD of 0.84 μm-sized tracer particles related to lag time at different peptide concentrations, determined by MPT, with dashed line having a slope corresponding to the critical diffusive exponent a_{crit} = 0.78. (b) Superposition of MSD as a function of peptide concentration. Critical gel concentration, c_{gel}, determined to be 1 mg mL^{-1}. Reproduced with permission from ref 48. Copyright 2017 American Chemical Society.

HIGH-THROUGHPUT USE AND AUTOMATION

Recently there has been a surge in high-throughput capabilities within the wet lab; MPT and DDM's use of low sample volumes has the potential to make them effective methods for carrying out high-throughput microrheological studies (Table 2). MPT has previously been used by Schultz et al. to elucidate a phase diagram of biomaterial hydrogelators, with a total of 73 samples studied by affixing glass capillaries to standard microscope slides and rapidly cycling samples during imaging.[8] Alternatively, microfluidics have also been utilized in combination with MPT to produce droplet-sized samples of varying compositions by varying inlet streams and then imaging the droplets in a nonflowing state.[22] Being able to replicate this process for other materials will accelerate materials discovery with respect to their phase behavior.

Table 2. Examples of MPT and DDM Applied in High-Throughput Setups for Biomaterials Characterization

HTP device/method	analysis	properties	no. of samples	refs
manual cycling of samples	MPT	gelation conditions	73 (8 per slide)	8
microfluidic device	MPT	viscosity	50−100	22
droplet-based microfluidic device	MPT	viscosity	40 per device	70
liquids handler, machine learning	MPT/DDM	gelation kinetics	63	9
manual cycling of samples	MPT/DDM	gelation kinetics	25 (5 per slide)	71

https://doi.org/10.1021/acsbiomaterials.2c00035
ACS Biomater. Sci. Eng. 2022, 8, 2747−2763

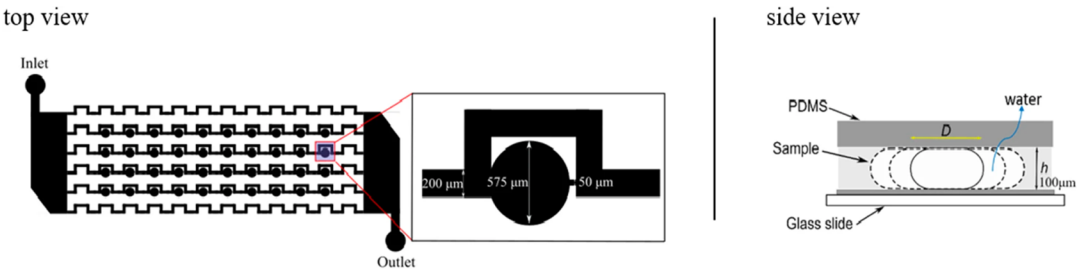

Figure 18. Top and side views of the microfluidic device used for microrheological measurements of viscosity. The side view shows decreasing droplet diameter as a result of water diffusing out through the PDMS layer, resulting in an increase in protein concentration in the aqueous slug. Reproduced with permission from ref 70. Copyright 2021 Springer Nature.

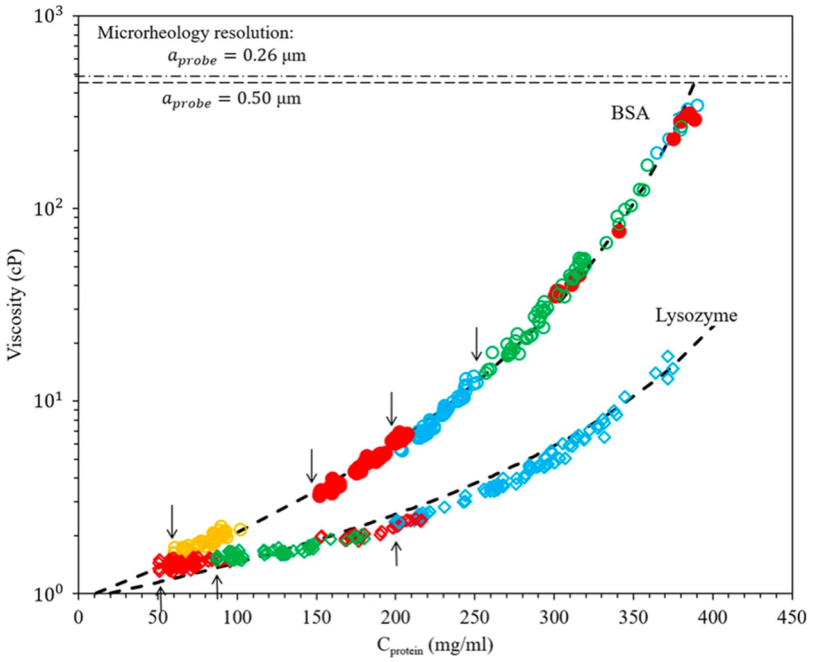

Figure 19. Viscosity measurements for BSA and lysozyme solutions across a range of concentrations determined by MPT. Each color in the figure represents one individual microfluidic device and the measurements made using it, with the loading concentration indicated by the arrow. Reproduced with permission from ref 70. Copyright 2021 Springer Nature.

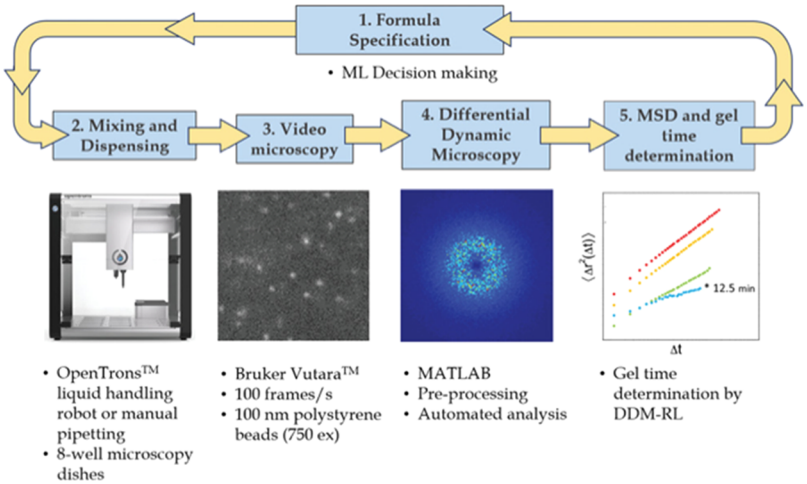

Figure 20. Pipeline used by Martineau et al. to make gelation time estimates and predict formulation conditions to yield silk hydrogels in desired time frames. Starting with a specific formulation (either an initial guess or one suggested by previous iterations), formulas were mixed and dispensed into eight-well plates. Series of images were acquired at set time points, with automated DDM analysis performed in *MATLAB*. DDM-RL was used as an estimate for gelation time, with outputs used to inform subsequent iterations. Reproduced with permission from ref 9. Copyright 2021 Wiley−VCH.

https://doi.org/10.1021/acsbiomaterials.2c00035
ACS Biomater. Sci. Eng. 2022, 8, 2747−2763

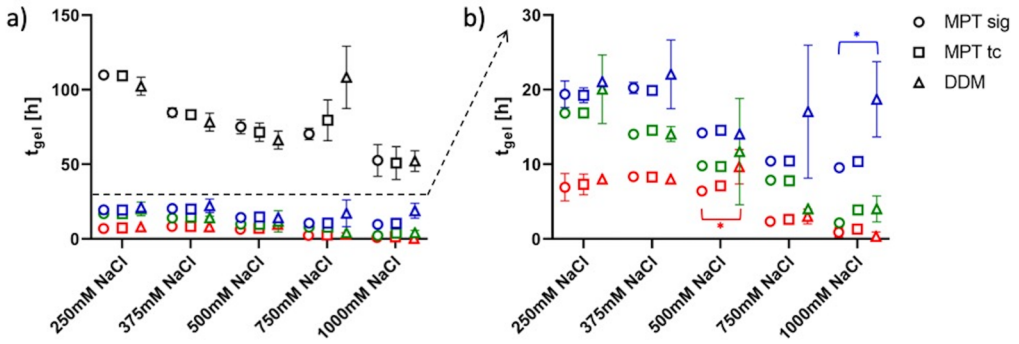

Figure 21. (a) Comparison of gelation times determined by fitting relaxation exponents from MPT to sigmoidal curves (MPT sig), by time−cure superposition (MPT tc), and by the last time point where the image structure function was resolvable for pH 7.4 (black), pH 10 (ref), pH 11 (green), and pH 12 (blue) at NaCl concentrations ranging from 250 to 1,000 mM. (b) Gelation times for pH 10−12 plotted on a smaller *y*-axis for better visualization of data trends. Reproduced with permission from ref 71. Copyright 2022 American Chemical Society.[71]

Yang et al. have also developed a droplet-based microfluidic device to quantify the viscosity of protein solutions over a range of protein concentrations.[70] This device utilized aqueous droplets containing different protein concentrations. The microfluidic device was made from polydimethylsiloxane (PDMS) and consisted of 40 nanoliter-sized droplet traps that had 575 μm diameters (Figure 18) and depth of 100 μm.[70] Each trap also had a 200 μm wide bypass channel and 50 μm wide restriction channel.[70] A slug of protein solution was injected into each trap with a continuous phase of mineral oil, after which viscosity and diameter of the protein droplets were assessed over time using MPT and microscopy, respectively, with dehydration of respective droplets resulting in the concentration of the protein over a range of hours.[70] This device was applied to model protein systems of BSA and lysozyme, showing that wide concentration and viscosity ranges can be studied using microliters of sample.[70] Specifically, microliters of sample were able to see concentration increases of 8× the original concentration and viscosity increases up to 2 orders of magnitude higher than the original viscosity, resulting in rapid viscosity measurements over a wide range of concentrations while using minimal sample (Figure 19).[70] This has potential applications in the pharmaceutical industry, where high dosage protein concentrations are needed for subcutaneous injection routes and are often associated with sharp increases in viscosity.[54,72]

Passive microrheology has already been automated with respect to the processing of collected images.[6,35] The data collection process itself also has potential to be automated through the use of motorized microscope stages that can quickly cycle through the different samples to be measured. Where microrheology lags in adaptation for high-throughput use is the dispensing of the sample into wells prior to measurement. Manual pipettors can lack precision and be user-dependent; automation of the dispensing process through autopipettors and robotic liquid handlers can further streamline the use of passive microrheology for high-throughput screening and eliminate sample-to-sample volume variability.

Martineau et al. have combined DDM microrheology with Bayesian machine learning algorithms in an automatable pipeline to tune the gelation time of an enzymatically cross-linked silk hydrogel with embedded *Escherichia coli* within a 4D parameter space (Figure 20).[9] This work serves as one of the initial forays in using DDM to analyze protein gelation kinetics and demonstrates some of the key strengths and weaknesses of DDM in analyzing gelation in a high-throughput, automatable fashion. Because DDM does not require user-optimization of analysis parameters before or during the image analysis, it is able to be applied in an automated set up.[9] The major weakness of using DDM in analyzing gelation kinetics is the difficulty in resolving MSD curves from samples where particles show small displacements.[9] Weak intensity fluctuations of confined particles' movement is on the same order as other contributions to the image structure function, such as the incoherent background contribution. To account for this, the resolution limit of DDM for MSD extraction (DDM-RL) was used as an estimate for gelation time, giving the pipeline a metric that can be determined in an automated analysis (Figure 20).[9] DDM-RL provides gel time estimates that are in general agreement with gelation times determined through conventionally used methods, such as $G' > G''$ crossover and time−cure superposition.[9] For the system reported, DDM-RL tends to underestimate gelation with respect to the estimates based on the time of the first observation, where $G' > G''$ over all measured frequencies. However, estimates of gel time by DDM are larger than the times indicated by time−cure superposition, indicating that DDM is sensitive to the particle motion associated with the low stiffness gels reacted past the critical extent.[9] In general, estimates between measurement approaches are within one or two observation intervals. Combining the automated assessment of gelation time with novel machine learning algorithms, Martineau and co-workers are able to identify regions within a 4D design space that are expected to gel within a targeted time frame of 5−15 min.[9]

Recently, the authors of this review compared the effectiveness of DDM and MPT in tracking gelation, using the previously described coiled-coil protein, Q,[11,73] as a model system.[71] Using an imaging setup similar to that of Schultz et al.,[8] 25 combinations of environmental conditions were screened for their effect on the gelation kinetics of Q.[71] Notably, this allowed for the rapid determination of an optimum at a pH near the isoelectric point and at the highest ionic strength within the range of conditions studied where gelation was observed on the shortest time scale.[71] This was used as a model case to compare the effectiveness of MPT and DDM in tracking gelation in high throughput. For MPT, gelation kinetics were analyzed using two methods; while the traditionally done time−cure superposition is a time-intensive, user-heavy process and thus not amenable for high-throughput implementation, relaxation exponents were also fit to sigmoidal curves such that analysis became automatable and user-bias was largely removed.[71] For DDM, the resolution limit

https://doi.org/10.1021/acsbiomaterials.2c00035
ACS Biomater. Sci. Eng. 2022, 8, 2747−2763

previously described by Martineau et al. was used as an estimate for the gelation time.[9] A key finding from this study, is that the methods largely agree with each other in determining gelation times of the protein at different environmental conditions (Figure 21). Although DDM is more amenable to high-throughput use due to its robust analysis and lack of user intervention, MPT also remains a key method because of its ability to track particle movement through the entire gelation process.[71] Thus, a possible combination of the two methods in assessing protein gelation kinetics may consist of using DDM to identify promising gelation conditions or variants within a library and then using MPT to fully elucidate the gelation kinetics and mechanism.

MPT and DDM lend themselves well to high-throughput screening and automation, as they can be employed using basic microscope setups and require less sample preparation compared to traditional microrheology. MPT has already been used in high-throughput for the characterization of a library of 73 samples in a single study, with the parallel nature of measurements favorable over serial measurements using traditional rheology.[8] However, thresholds used in MPT analysis may need to be optimized and recalibrated between samples, making MPT better suited to libraries of samples that have similar properties. Alternatively, DDM may be able to study a wider range of samples within the same experiment due to the smaller number of user-defined inputs.[9] In both cases, it is possible to automate the data analysis, placing the bottleneck of high-throughput measurements on the time it takes for imaging. For time-sensitive measurements such as gelation reactions, the throughput of data collection is likely to be limited further based on how reasonable the assumption is that the system does not undergo significant evolution during the measurement.

CONCLUSIONS AND FUTURE PERSPECTIVES

Microrheology is a powerful tool for the characterization of biomaterials and their properties. Although initial methods included MPT and DWS,[44] new methods of passive and active microrheology continue to be developed. The passive microrheology techniques of MPT and DDM have been highlighted in this review for their ease of use and application. The use of small sample volumes as well as the ability to make *in situ* measurements make it possible to screen a large number of samples in parallel, significantly increasing throughput compared to oscillatory shear rheology. Although already useful in the characterization of soft materials, the potential for automation and high-throughput application can further accelerate the research and development of novel protein biomaterials.

Passive microrheology is thus a useful part of the protein engineering toolbox, having the potential to rapidly screen a number of samples for materials whose sample preparation can often be costly and time consuming. Thus far, applications of MPT and DDM range from determining properties such as viscosities and viscoelastic moduli to tracking the self-assembly of proteins into fibers and hierarchical structures such as hydrogels. Additionally, these methods can be used to study the heterogeneity of a material's microenvironment. Rapid acquisition of this information can be serviceable in the characterization of new protein libraries.

AUTHOR INFORMATION

Corresponding Author

Jin Kim Montclare − *Department of Chemical and Biomolecular Engineering, Tandon School of Engineering, New York University, New York, New York 11201, United States; Department of Radiology, New York University Langone Health, New York, New York 10016, United States; Department of Biomaterials, College of Dentistry, New York University, New York, New York 10010, United States; Department of Chemistry, New York University, New York, New York 10003, United States;* orcid.org/0000-0001-6857-3591; Email: montclare@nyu.edu

Authors

Michael Meleties − *Department of Chemical and Biomolecular Engineering, Tandon School of Engineering, New York University, New York, New York 11201, United States*

Rhett L. Martineau − *Materials and Manufacturing Directorate, Air Force Research Laboratory, Wright-Patterson AFB, Ohio 45433, United States; Biological and Nanoscale Technologies Division, UES Inc., Dayton, Ohio 45432, United States*

Maneesh K. Gupta − *Materials and Manufacturing Directorate, Air Force Research Laboratory, Wright-Patterson AFB, Ohio 45433, United States*

Complete contact information is available at: https://pubs.acs.org/10.1021/acsbiomaterials.2c00035

Author Contributions

The manuscript was written through contributions of all authors. All authors have given approval to the final version of the manuscript.

Funding

This work was supported by NSF-DMREF under Award DMR 1728858.

Notes

The authors declare no competing financial interest.

REFERENCES

(1) Macosko, C. W. *Rheology: Principles, Measurements, and Applications*; Wiley−VCH, 1994.

(2) Mitchell, J. R. The Rheology of Gels. *Journal of Texture Studies* **1980**, *11* (4), 315−337.

(3) Waigh, T. A. Microrheology of complex fluids. *Rep. Prog. Phys.* **2005**, *68* (3), 685.

(4) Waigh, T. A. Advances in the microrheology of complex fluids. *Rep. Prog. Phys.* **2016**, *79* (7), 074601.

(5) Larsen, T.; Schultz, K.; Furst, E. M. Hydrogel microrheology near the liquid-solid transition. *Korea-Austr. Rheol. J.* **2008**, *20* (3), 165−173.

(6) Larsen, T. H.; Furst, E. M. Microrheology of the Liquid-Solid Transition during Gelation. *Phys. Rev. Lett.* **2008**, *100* (14), 146001.

(7) Squires, T. M.; Mason, T. G. Fluid Mechanics of Microrheology. *Annu. Rev. Fluid Mech.* **2010**, *42* (1), 413−438.

(8) Schultz, K. M.; Baldwin, A. D.; Kiick, K. L.; Furst, E. M. Rapid rheological screening to identify conditions of biomaterial hydrogelation. *Soft Matter* **2009**, *5* (4), 740−742.

(9) Martineau, R. L.; Bayles, A. V.; Hung, C.-S.; Reyes, K. G.; Helgeson, M. E.; Gupta, M. K. Engineering Gelation Kinetics in Living Silk Hydrogels by Differential Dynamic Microscopy Microrheology and Machine Learning. *Adv. Biol. (Weinh)* **2021**, *6*, e2101070.

(10) Regan, K.; Wulstein, D.; Rasmussen, H.; McGorty, R.; Robertson-Anderson, R. M. Bridging the spatiotemporal scales of macromolecular transport in crowded biomimetic systems. *Soft Matter* **2019**, *15* (6), 1200−1209.
(11) Hill, L. K.; Meleties, M.; Katyal, P.; Xie, X.; Delgado-Fukushima, E.; Jihad, T.; Liu, C.-F.; O'Neill, S.; Tu, R. S.; Renfrew, P. D.; Bonneau, R.; Wadghiri, Y. Z.; Montclare, J. K. Thermoresponsive Protein-Engineered Coiled-Coil Hydrogel for Sustained Small Molecule Release. *Biomacromolecules* **2019**, *20* (9), 3340−3351.
(12) Larsen, T. H.; Branco, M. C.; Rajagopal, K.; Schneider, J. P.; Furst, E. M. Sequence-Dependent Gelation Kinetics of β-Hairpin Peptide Hydrogels. *Macromolecules* **2009**, *42* (21), 8443−8450.
(13) Zaner, K. S.; Valberg, P. A. Viscoelasticity of F-actin measured with magnetic microparticles. *J. Cell Biol.* **1989**, *109* (5), 2233−2243.
(14) Helfer, E.; Harlepp, S.; Bourdieu, L.; Robert, J.; MacKintosh, F. C.; Chatenay, D. Microrheology of Biopolymer-Membrane Complexes. *Phys. Rev. Lett.* **2000**, *85* (2), 457−460.
(15) Veigel, C.; Bartoo, M. L.; White, D. C. S.; Sparrow, J. C.; Molloy, J. E. The Stiffness of Rabbit Skeletal Actomyosin Cross-Bridges Determined with an Optical Tweezers Transducer. *Biophys. J.* **1998**, *75* (3), 1424−1438.
(16) Alcaraz, J.; Buscemi, L.; Grabulosa, M.; Trepat, X.; Fabry, B.; Farré, R.; Navajas, D. Microrheology of Human Lung Epithelial Cells Measured by Atomic Force Microscopy. *Biophys. J.* **2003**, *84* (3), 2071−2079.
(17) Mahaffy, R. E.; Shih, C. K.; MacKintosh, F. C.; Käs, J. Scanning Probe-Based Frequency-Dependent Microrheology of Polymer Gels and Biological Cells. *Phys. Rev. Lett.* **2000**, *85* (4), 880−883.
(18) Okajima, T.; Arakawa, H.; Taufiq Alam, M.; Sekiguchi, H.; Ikai, A. Dynamics of a partially stretched protein molecule studied using an atomic force microscope. *Biophys. Chem.* **2004**, *107* (1), 51−61.
(19) Zia, R. N. Active and Passive Microrheology: Theory and Simulation. *Annu. Rev. Fluid Mech.* **2018**, *50* (1), 371−405.
(20) Yao, A.; Tassieri, M.; Padgett, M.; Cooper, J. Microrheology with optical tweezers. *Lab Chip* **2009**, *9* (17), 2568−2575.
(21) Efremov, Y. M.; Okajima, T.; Raman, A. Measuring viscoelasticity of soft biological samples using atomic force microscopy. *Soft Matter* **2020**, *16* (1), 64−81.
(22) Schultz, K. M.; Furst, E. M. Microrheology of biomaterial hydrogelators. *Soft Matter* **2012**, *8* (23), 6198−6205.
(23) Kastantin, M.; Walder, R.; Schwartz, D. K. Identifying mechanisms of interfacial dynamics using single-molecule tracking. *Langmuir* **2012**, *28* (34), 12443−12456.
(24) Hassan, P. A.; Rana, S.; Verma, G. Making sense of Brownian motion: colloid characterization by dynamic light scattering. *Langmuir* **2015**, *31* (1), 3−12.
(25) Joyner, K.; Yang, S.; Duncan, G. A. Microrheology for biomaterial design. *APL Bioengineering* **2020**, *4* (4), 041508.
(26) McGlynn, J. A.; Wu, N.; Schultz, K. M. Multiple particle tracking microrheological characterization: Fundamentals, emerging techniques and applications. *J. Appl. Phys.* **2020**, *127* (20), 201101.
(27) Dufresne, E. R.; Squires, T. M.; Brenner, M. P.; Grier, D. G. Hydrodynamic Coupling of Two Brownian Spheres to a Planar Surface. *Phys. Rev. Lett.* **2000**, *85* (15), 3317−3320.
(28) Bayles, A. V.; Squires, T. M.; Helgeson, M. E. Dark-field differential dynamic microscopy. *Soft Matter* **2016**, *12* (8), 2440−2452.
(29) Cerbino, R.; Giavazzi, F.; Helgeson, M. E. Differential dynamic microscopy for the characterization of polymer systems. *J. Polym. Sci.* **2021**, *60* (7), 1−11.
(30) Cerbino, R.; Trappe, V. Differential Dynamic Microscopy: Probing Wave Vector Dependent Dynamics with a Microscope. *Phys. Rev. Lett.* **2008**, *100* (18), 188102.
(31) Katyal, P.; Meleties, M.; Montclare, J. K. Self-Assembled Protein- and Peptide-Based Nanomaterials. *ACS Biomaterials Science & Engineering* **2019**, *5* (9), 4132−4147.
(32) Liu, W.; Wu, C. Rheological study of soft matters: A review of microrheology and microrheometers. *Macromol. Chem. Phys.* **2018**, *219* (3), 1700307.
(33) Cicuta, P.; Donald, A. M. Microrheology: a review of the method and applications. *Soft Matter* **2007**, *3* (12), 1449−1455.
(34) Crocker, J. C.; Grier, D. G. Methods of Digital Video Microscopy for Colloidal Studies. *J. Colloid Interface Sci.* **1996**, *179* (1), 298−310.
(35) Bayles, A. V.; Squires, T. M.; Helgeson, M. E. Probe microrheology without particle tracking by differential dynamic microscopy. *Rheol. Acta* **2017**, *56* (11), 863−869.
(36) Mason, T. G.; Ganesan, K.; van Zanten, J. H.; Wirtz, D.; Kuo, S. C. Particle Tracking Microrheology of Complex Fluids. *Phys. Rev. Lett.* **1997**, *79* (17), 3282−3285.
(37) Kegel, W. K.; van Blaaderen, A. Direct observation of dynamical heterogeneities in colloidal hard-sphere suspensions. *Science* **2000**, *287* (5451), 290−293.
(38) Furst, E. M.; Squires, T. M. *Microrheology*; Oxford University Press, 2017.
(39) Crocker, J. C.; Valentine, M. T.; Weeks, E. R.; Gisler, T.; Kaplan, P. D.; Yodh, A. G.; Weitz, D. A. Two-point microrheology of inhomogeneous soft materials. *Phys. Rev. Lett.* **2000**, *85* (4), 888.
(40) Pelletier, V.; Gal, N.; Fournier, P.; Kilfoil, M. L. Microrheology of Microtubule Solutions and Actin-Microtubule Composite Networks. *Phys. Rev. Lett.* **2009**, *102* (18), 188303.
(41) Richards, J. A.; Martinez, V. A.; Arlt, J. Particle sizing for flowing colloidal suspensions using flow-differential dynamic microscopy. *Soft Matter* **2021**, *17* (14), 3945−3953.
(42) Edera, P.; Bergamini, D.; Trappe, V.; Giavazzi, F.; Cerbino, R. Differential dynamic microscopy microrheology of soft materials: A tracking-free determination of the frequency-dependent loss and storage moduli. *Physical Review Materials* **2017**, *1* (7), 073804.
(43) Cerbino, R.; Cicuta, P. Perspective: Differential dynamic microscopy extracts multi-scale activity in complex fluids and biological systems. *J. Chem. Phys.* **2017**, *147* (11), 110901.
(44) Pine, D. J.; Weitz, D. A.; Chaikin, P. M.; Herbolzheimer, E. Diffusing wave spectroscopy. *Phys. Rev. Lett.* **1988**, *60* (12), 1134−1137.
(45) Martinez, V. A.; Besseling, R.; Croze, O. A.; Tailleur, J.; Reufer, M.; Schwarz-Linek, J.; Wilson, L. G.; Bees, M. A.; Poon, W. C.K. Differential Dynamic Microscopy: A High-Throughput Method for Characterizing the Motility of Microorganisms. *Biophys. J.* **2012**, *103* (8), 1637−1647.
(46) Jepson, A.; Arlt, J.; Statham, J.; Spilman, M.; Burton, K.; Wood, T.; Poon, W. C. K.; Martinez, V. A. High-throughput characterisation of bull semen motility using differential dynamic microscopy. *PLoS One* **2019**, *14* (4), e0202720.
(47) Tu, R. S.; Breedveld, V. Microrheological detection of protein unfolding. *Phys. Rev. E* **2005**, *72* (4), 041914.
(48) Zhou, Y.; Li, B.; Li, S.; Ardoña, H. A. M.; Wilson, W. L.; Tovar, J. D.; Schroeder, C. M. Concentration-Driven Assembly and Sol−Gel Transition of π-Conjugated Oligopeptides. *ACS Central Science* **2017**, *3* (9), 986−994.
(49) Safari, M. S.; Vorontsova, M. A.; Poling-Skutvik, R.; Vekilov, P. G.; Conrad, J. C. Differential dynamic microscopy of weakly scattering and polydisperse protein-rich clusters. *Phys. Rev. E* **2015**, *92* (4), 042712.
(50) He, K.; Spannuth, M.; Conrad, J. C.; Krishnamoorti, R. Diffusive dynamics of nanoparticles in aqueous dispersions. *Soft Matter* **2012**, *8* (47), 11933−11938.
(51) Roth, A.; Murschel, F.; Latreille, P.-L.; Martinez, V. A.; Liberelle, B.; Banquy, X.; De Crescenzo, G. Coiled Coil Affinity-Based Systems for the Controlled Release of Biofunctionalized Gold Nanoparticles from Alginate Hydrogels. *Biomacromolecules* **2019**, *20* (5), 1926−1936.
(52) Heinen, M.; Zanini, F.; Roosen-Runge, F.; Fedunová, D.; Zhang, F.; Hennig, M.; Seydel, T.; Schweins, R.; Sztucki, M.; Antalík, M.; et al. Viscosity and diffusion: crowding and salt effects in protein solutions. *Soft Matter* **2012**, *8* (5), 1404−1419.
(53) Jezek, J.; Rides, M.; Derham, B.; Moore, J.; Cerasoli, E.; Simler, R.; Perez-Ramirez, B. Viscosity of concentrated therapeutic protein

https://doi.org/10.1021/acsbiomaterials.2c00035
ACS Biomater. Sci. Eng. 2022, 8, 2747−2763

compositions. *Advanced drug delivery reviews* **2011**, *63* (13), 1107−1117.
(54) Josephson, L. L.; Furst, E. M.; Galush, W. J. Particle tracking microrheology of protein solutions. *J. Rheol.* **2016**, *60* (4), 531−540.
(55) Escobedo-Sánchez, M. A.; Segovia-Gutiérrez, J. P.; Zuccolotto-Bernez, A. B.; Hansen, J.; Marciniak, C. C.; Sachowsky, K.; Platten, F.; Egelhaaf, S. U. Microliter viscometry using a bright-field microscope: *η*-DDM. *Soft Matter* **2018**, *14* (34), 7016−7025.
(56) Fisher, R. S.; Elbaum-Garfinkle, S. Tunable multiphase dynamics of arginine and lysine liquid condensates. *Nat. Commun.* **2020**, *11* (1), 4628.
(57) A. Bos, M.; van Vliet, T. Interfacial rheological properties of adsorbed protein layers and surfactants: a review. *Adv. Colloid Interface Sci.* **2001**, *91* (3), 437−471.
(58) Lee, M. H.; Reich, D. H.; Stebe, K. J.; Leheny, R. L. Combined Passive and Active Microrheology Study of Protein-Layer Formation at an Air−Water Interface. *Langmuir* **2010**, *26* (4), 2650−2658.
(59) Yang, N.; Ye, J.; Li, J.; Hu, B.; Leheny, R. L.; Nishinari, K.; Fang, Y. Interfacial behaviour of *β*-lactoglobulin aggregates at the oil−water interface studied using particle tracking and dilatational rheology. *Soft Matter* **2021**, *17* (10), 2973−2984.
(60) Schultz, K. M.; Baldwin, A. D.; Kiick, K. L.; Furst, E. M. Gelation of covalently cross-linked PEG− heparin hydrogels. *Macromolecules* **2009**, *42* (14), 5310−5316.
(61) Winter, H. H.; Chambon, F. Analysis of linear viscoelasticity of a crosslinking polymer at the gel point. *J. Rheol.* **1986**, *30* (2), 367−382.
(62) Katyal, P.; Hettinghouse, A.; Meleties, M.; Hasan, S.; Chen, C.; Cui, M.; Sun, G.; Menon, R.; Lin, B.; Regatte, R.; Montclare, J. K.; Liu, C.-j. Injectable recombinant block polymer gel for sustained delivery of therapeutic protein in post traumatic osteoarthritis. *Biomaterials* **2022**, *281*, 121370.
(63) Xia, X.-X.; Xu, Q.; Hu, X.; Qin, G.; Kaplan, D. L. Tunable self-assembly of genetically engineered silk−elastin-like protein polymers. *Biomacromolecules* **2011**, *12* (11), 3844−3850.
(64) Aufderhorst-Roberts, A.; Frith, W. J.; Donald, A. M. A microrheological study of hydrogel kinetics and micro-heterogeneity. *Eur. Phys. J. E* **2014**, *37* (5), 44.
(65) Frith, W. J.; Donald, A. M.; Adams, D. J.; Aufderhorst-Roberts, A. Gels formed from amino-acid derivatives, their novel rheology as probed by bulk and particle tracking rheological methods. *J. Non-Newtonian Fluid Mech.* **2015**, *222*, 104−111.
(66) Levin, M.; Sorkin, R.; Pine, D.; Granek, R.; Bernheim-Groswasser, A.; Roichman, Y. Kinetics of actin networks formation measured by time resolved particle-tracking microrheology. *Soft Matter* **2020**, *16* (33), 7869−7876.
(67) Meldrum, O. W.; Yakubov, G. E.; Bonilla, M. R.; Deshmukh, O.; McGuckin, M. A.; Gidley, M. J. Mucin gel assembly is controlled by a collective action of non-mucin proteins, disulfide bridges, Ca 2+-mediated links, and hydrogen bonding. *Sci. Rep.* **2018**, *8* (1), 1−16.
(68) Joyner, K.; Song, D.; Hawkins, R. F.; Silcott, R. D.; Duncan, G. A. A rational approach to form disulfide linked mucin hydrogels. *Soft Matter* **2019**, *15* (47), 9632−9639.
(69) Yonemoto, J.; Maki, Y.; Koh, I.; Furusawa, K.; Annaka, M. Formation of Multi-Channel Collagen Gels Investigated Using Particle Tracking Microrheology. *Biomacromolecules* **2021**, *22* (9), 3819−3826.
(70) Yang, D.; Daviran, M.; Schultz, K. M.; Walker, L. M. Droplet-Based Microfluidic Tool to Quantify Viscosity of Concentrating Protein Solutions. *Pharm. Res.* **2021**, *38* (10), 1765−1775.
(71) Meleties, M.; Britton, D.; Katyal, P.; Lin, B.; Martineau, R. L.; Gupta, M. K.; Montclare, J. K. High-Throughput Microrheology for the Assessment of Protein Gelation Kinetics. *Macromolecules* **2022**, *55*, 1239.
(72) Yadav, S.; Shire, S. J.; Kalonia, D. S. Factors affecting the viscosity in high concentration solutions of different monoclonal antibodies. *Journal of pharmaceutical sciences* **2010**, *99* (12), 4812−4829.
(73) Meleties, M.; Katyal, P.; Lin, B.; Britton, D.; Montclare, J. K. Self-assembly of stimuli-responsive coiled-coil fibrous hydrogels. *Soft Matter* **2021**, *17* (26), 6470−6476.

https://doi.org/10.1021/acsbiomaterials.2c00035
ACS Biomater. Sci. Eng. 2022, 8, 2747−2763